

Second order semi-parametric inference for multivariate log Gaussian Cox processes

Kristian Bjørn Hessellund

Department of Mathematical Sciences, Aalborg University, Denmark

Ganggang Xu

Department of Management Science, University of Miami, USA

Yongtao Guan

Department of Management Science, University of Miami, USA

Rasmus Waagepetersen

Department of Mathematical Sciences, Aalborg University, Denmark

†E-mail: rw@math.aau.dk

Summary.

This paper introduces a new approach to inferring the second order properties of a multivariate log Gaussian Cox process (LGCP) with a complex intensity function. We assume a semi-parametric model for the multivariate intensity function containing an unspecified complex factor common to all types of points. Given this model we construct a second-order conditional composite likelihood to infer the pair correlation and cross pair correlation functions of the LGCP. Crucially this likelihood does not depend on the unspecified part of the intensity function. We also introduce a cross validation method for model selection and an algorithm for regularized inference that can be used to obtain sparse models for cross pair correlation functions. The methodology is applied to simulated data as well as data examples from microscopy and criminology. This shows how the new approach outperforms existing alternatives where the intensity functions are estimated non-parametrically.

Keywords: case-control, composite likelihood, conditional likelihood, cross pair correlation function, multivariate, pair correlation function, point process.

1. Introduction

A multivariate or multi-type point pattern is a marked point pattern where the marks belong to a finite set corresponding to different types of points. Equivalently, a multivariate point pattern can be viewed as a finite collection of ordinary point patterns, where each of these point patterns consists of points of a specific type. In this paper we consider point pattern data from biology and criminology. In the

†*Address for correspondence:* Department of Mathematical Sciences, Aalborg University, Skjernvej 4A, DK-9220 Aalborg

former case the point pattern represents locations of different types of cells in a tumor and in the latter case, crime scenes of different types of crimes. An obvious key point of interest is then to study possible associations between the points of different types.

If consistent estimates of the intensity functions are available, and assuming second-order intensity reweighted stationarity (Baddeley et al., 2000) or intensity-reweighted moment stationarity (van Lieshout, 2011), an immediate approach is to compute non-parametric cross summary statistics such as cross K , cross pair correlation, or cross J functions (Møller and Waagepetersen, 2003; Baddeley et al., 2014; Cronie and van Lieshout, 2016). Parametric estimation of cross associations is also possible. Jalilian et al. (2015), Waagepetersen et al. (2016) and Choiruddin et al. (2019) used parametric models of intensity and pair correlation functions, while Rajala et al. (2018) specified a full multivariate Markov point process model.

In some cases it is not straightforward to estimate the intensity function. For the cells data, the intensities of each type appear to be very heterogeneous, possibly varying within regions corresponding to different types of tissue. However, it is not straightforward to delineate these regions. For the crime data, the intensity functions depend in a complex manner on the urban structures and the population density.

In case of bivariate case-control processes, Diggle et al. (2007) suggested a semi-parametric model where complex features of the case and control intensity functions were captured by a common non-parametric factor. This factor was estimated non-parametrically from the control point process and next used in a semi-parametric estimate of the intensity function for the case process. Finally this estimate was plugged into an estimate of the K -function for the case process. This estimation method mitigates the problem of confounding of clustering in the case process with variations in the case intensity function. However, sensitivity to the choice of bandwidth for the non-parametric estimation remains. Also the case and control processes were assumed to be independent whereby the cross pair correlation function is restricted to be one. Diggle et al. (2007) assumed the control process to be Poisson and Henrys and Brown (2009) relaxed this assumption by allowing both case and control processes to be clustered. They however retained independence between the two processes. Guan et al. (2008) used the same framework as Diggle et al. (2007) but used a second-order conditional composite likelihood to fit a parametric model to the case pair correlation function. The composite likelihood notably did not depend on the non-parametric part of the case intensity function and hence avoided choosing a bandwidth for non-parametric estimation. In the same case-control setting, Xu et al. (2019) introduced an optimal stochastic quasi-likelihood function for estimating the parametric component of the intensity function for the cases.

In the context of multivariate point processes, Hessellund et al. (2021) used a semi-parametric model for the multivariate intensity function. They assumed a multiplicative structure where for each type of points, the intensity function is a product of a common background intensity and a log-linear factor modeling effects of covariates. Hence focus is on estimating differences between the intensity functions (for different types of points) that can be explained in terms of the covariates. In the bivariate case this model coincides with the one used in Diggle et al. (2007) and Xu

et al. (2019). However, Hessellund et al. (2021) did not impose any restrictive assumptions regarding the correlations within each type of points or between different types of points. While the main focus in Hessellund et al. (2021) was inference for the intensity function, they also obtained non-parametric estimates of ratios of cross pair correlation functions. They were, however, not able to obtain estimates of the individual cross pair correlation functions. Xu et al. (2020) obtained a consistent estimate of a common pair correlation function in presence of a common completely unspecified intensity function but they considered the particular multivariate setting of independent and identically distributed point processes.

Our objective in this paper is to infer the full within and between correlation structure of a multivariate point process. To do so we adopt the parametric log Gaussian Cox process (LGCP) model for the correlation structure proposed in Waagepetersen et al. (2016) and further considered in Choiruddin et al. (2019). This model is flexible and has a very natural interpretation in terms of latent structures. However, to deal with complex intensity functions, we replace the parametric model for the intensity function used in Waagepetersen et al. (2016) with the semi-parametric model for the intensity function from Hessellund et al. (2021). In this way we combine the strengths of two modelling approaches.

The presence of a non-parametric factor in the intensity function means that ingenuity is needed for fitting the parametric part of the model. We generalize the approach for the bivariate case in Guan et al. (2008) and obtain a second order conditional composite likelihood function. This only depends on the parametric parts of the model and does not require knowledge of the non-parametric component. Compared with Guan et al. (2008), we consider an arbitrary number of point processes and do not assume that any of the point processes are Poisson, nor that any two point processes are uncorrelated.

Some key questions we want to address for a particular data set are whether some point processes are uncorrelated and if not, whether they are negatively or positively correlated. We address these questions by a model selection approach where the models considered represent different types of correlation structures. Absence of correlation between point processes requires that certain parameters must be zero. To enable selection of models with parameters set to zero we combine our semi-parametric composite likelihood with a Lasso penalization (Tibshirani, 1996). This precisely facilitates that some parameters can be estimated to be exactly zero. A similar approach was considered by Choiruddin et al. (2019) in the context of least squares estimation for a multivariate LGCP with a full parametric model for the multivariate intensity function.

The rest of the paper is organized as follows. Section 2 gives a brief overview of multivariate point processes with focus on the intensity functions and cross intensity functions. Next, the semi-parametric model for the intensity function and the multivariate LGCP model is described. Section 3 introduces the second order conditional composite likelihood function, an optimization algorithm based on the proximal Newton method, and a cross validation method for model selection. Section 4 contains simulation studies and Section 5 applies our methodology to cells and crimes data sets. Some concluding remarks are given in Section 6.

2. Semi-parametric modelling of a multivariate point process

2.1. Background on intensity functions

Let $\mathbf{X} = (X_1, \dots, X_p)$ be a multivariate spatial point process, where X_i is a spatial point process on \mathbb{R}^d representing points of type i , $i = 1, \dots, p$. Each X_i is hence a random subset of \mathbb{R}^d such that the cardinality of $X_i \cap B$ is finite almost surely for any bounded $B \subset \mathbb{R}^d$. We observe \mathbf{X} in a spatial window W , where the window $W \subset \mathbb{R}^d$ is bounded with area $|W| > 0$. We will assume there exist for each $i, j = 1, \dots, p$, non-negative functions $\rho_i(\cdot)$ and $\rho_{ij}(\cdot)$ so that the so-called Campbell's formulae:

$$\mathbb{E} \sum_{\mathbf{u} \in X_i} h_1(\mathbf{u}) = \int h_1(\mathbf{u}) \rho_i(\mathbf{u}) d\mathbf{u} \quad (1)$$

$$\mathbb{E} \sum_{\substack{\neq \\ \mathbf{u} \in X_i, \mathbf{v} \in X_j}} h_2(\mathbf{u}, \mathbf{v}) = \int h_2(\mathbf{u}, \mathbf{v}) \rho_{ij}(\mathbf{u}, \mathbf{v}) d\mathbf{u} d\mathbf{v}, \quad (2)$$

hold for any non-negative functions $h_1(\cdot)$ and $h_2(\cdot, \cdot)$. Here \sum^{\neq} means sum over pairwise distinct pairs (\mathbf{u}, \mathbf{v}) . The function $\rho_i(\cdot)$ is called the intensity function of X_i . If $i = j$, then $\rho_{ii}(\cdot)$ is called the second order intensity function of X_i , while if $i \neq j$, $\rho_{ij}(\cdot)$ is called the cross intensity function between X_i and X_j . The normalized cross intensity function, called cross pair correlation function (cross PCF), is denoted $g_{ij}(\cdot)$ and defined by: $\rho_i(\mathbf{u}) \rho_j(\mathbf{v}) g_{ij}(\mathbf{u}, \mathbf{v}) = \rho_{ij}(\mathbf{u}, \mathbf{v})$. If $i = j$ we just call $g_{ii}(\cdot)$ the pair correlation function (PCF) for X_i . If X_i and X_j are independent, then $g_{ij}(\mathbf{u}, \mathbf{v}) = 1$. The case $g_{ij}(\mathbf{u}, \mathbf{v}) > 1$ (< 1) is indicative of positive (negative) association between X_i and X_j (or between points in X_i in the case $i = j$). Hence the cross PCFs provide useful insight regarding the dependence within and between the point processes. We assume that X is second order cross intensity reweighted stationary and isotropic, i.e., with an abuse of notation, $g_{ij}(\mathbf{u}, \mathbf{v}) = g_{ij}(r)$, $i, j = 1, \dots, p$, where $r = \|\mathbf{u} - \mathbf{v}\|$.

2.2. Semi-parametric regression model for the intensity

It may sometimes be difficult to specify a simple parametric model for the intensity functions. One may then resort to non-parametric estimation of the intensity functions. The results then depend heavily on the choice of smoothing bandwidth where different data driven methods may result in very different results, see e.g. simulation studies in Cronie and van Lieshout (2018) and Shaw et al. (2020). We instead consider a semi-parametric model where a background intensity function $\rho_0(\cdot)$ captures complex variation in the intensity functions that is common to all the point processes X_1, \dots, X_p . For the cells data considered in Section 5.1, $\rho_0(\cdot)$ may capture variations in tissue composition that influence occurrence of different types of cells. For the crime data in Section 5.2, $\rho_0(\cdot)$ captures variation in population density and dependence of the intensities on the urban structure. More specifically, following Hessellund et al. (2021), we consider the multiplicative model:

$$\rho_i(\mathbf{u}; \boldsymbol{\gamma}_i) = \rho_0(\mathbf{u}) \exp(\boldsymbol{\gamma}_i^\top \mathbf{z}(\mathbf{u})) \quad (3)$$

for the intensity of X_i , where $\mathbf{z}(\mathbf{u})$ denotes a vector of spatial covariates at location \mathbf{u} and $\boldsymbol{\gamma}_i$ is a regression parameter vector. Let $\rho^{\text{pooled}} = \sum_{i=1}^p \rho_i$ denote the intensity of the pooled point process $X^{\text{pooled}} = \cup_{i=1}^p X_i$. The intensity function ρ_i can then be decomposed in a natural way as $\rho^{\text{pooled}}(\cdot) p_i(\cdot; \boldsymbol{\gamma}_i)$ where $p_i(\mathbf{u}; \boldsymbol{\gamma}_i) = \rho_i(\mathbf{u}; \boldsymbol{\gamma}_i) / \rho^{\text{pooled}}(\mathbf{u})$ is the conditional probability that a point \mathbf{u} is of type i given that $\mathbf{u} \in X^{\text{pooled}}$.

The parameters $\boldsymbol{\gamma}_i$ are not identifiable: replacing the l th entry γ_{il} in $\boldsymbol{\gamma}_i$ by $\gamma_{il} - K$ for $i = 1, \dots, p$ while replacing $\rho_0(\cdot)$ by $\rho_0(\cdot) \exp(K z_l(\mathbf{u}))$ does not change the model when $\rho_0(\cdot)$ is unspecified. Hesselund et al. (2021) proposed a first order conditional composite likelihood for estimating contrasts $\boldsymbol{\beta}_i = \boldsymbol{\gamma}_i - \boldsymbol{\gamma}_p$. The first order conditional composite likelihood was obtained as the product $\prod_{i=1}^p \prod_{\mathbf{u} \in X_i} p_i(\mathbf{u}; \boldsymbol{\beta}_i)$ with the constraint $\boldsymbol{\beta}_p = \mathbf{0}$. Alternatively, one could impose sum-to-zero constraints $\sum_{i=1}^p \boldsymbol{\beta}_i = \mathbf{0}$ on the $\boldsymbol{\beta}_i$.

Given the semi-parametric model for the intensity functions and its associated estimation procedure we specify in the next section a model for the correlation structure of the multivariate point process.

2.3. Multivariate log Gaussian Cox model

Following the setup in Waagepetersen et al. (2016), we assume that X_i for $i = 1, \dots, p$, is a Cox process with random intensity function:

$$\Lambda_i(\mathbf{u}) = \rho_0(\mathbf{u}) \exp(\boldsymbol{\gamma}_i^\top \mathbf{z}(\mathbf{u})) \exp\left(\mu_i + \sum_{k=1}^q \alpha_{ik} Y_k(\mathbf{u}) + \sigma_i U_i(\mathbf{u})\right), \quad (4)$$

where the Y_k and U_i are independent zero mean unit variance Gaussian random fields and $\mu_i = -\sum_{k=1}^q \alpha_{ik}^2 / 2 - \sigma_i^2 / 2$. We interpret the Y_k as latent random factors that influence all types of points. Hence the different types of points may be correlated due to dependence on the Y_k . Moreover, each U_i is a type-specific random factor that only affects the i th type of points. Hence U_i models random clustering within each X_i .

Consider for a moment the ideal situation where the Y_k are observed (non-random). Following the same considerations as for the $\boldsymbol{\gamma}_i$ in the previous section we should then impose restrictions $\alpha_{pl} = 0$ or $\sum_{i=1}^p \alpha_{il} = 0$, $l = 1, \dots, q$, in order to ensure identifiability. In case of unobserved Y_k and hence less information, the need for a constraint is not less pertinent. In the following we impose the sum-to-zero constraint $\sum_{i=1}^p \alpha_{il} = 0$, $l = 1, \dots, q$ which treats all X_i symmetrically.

The intensity function of X_i is $\rho_i(\mathbf{u}) = \mathbb{E}[\Lambda_i(\mathbf{u})] = \rho_0(\mathbf{u}) \exp(\boldsymbol{\gamma}_i^\top \mathbf{z}(\mathbf{u}))$, which follows from the moment generating function of a Gaussian random variable. Similarly,

$$\begin{aligned} \rho_{ij}(\mathbf{u}, \mathbf{v}) &= \mathbb{E}[\Lambda_i(\mathbf{u}) \Lambda_j(\mathbf{v})] = \rho_0(\mathbf{u}) \rho_0(\mathbf{v}) \exp(\boldsymbol{\gamma}_i^\top \mathbf{z}(\mathbf{u})) \exp(\boldsymbol{\gamma}_j^\top \mathbf{z}(\mathbf{v})) \\ &\quad \times \exp\left(\sum_{k=1}^q \alpha_{ik} \alpha_{jk} c_{Y_k}(\mathbf{u}, \mathbf{v}) + 1[i=j] \sigma_i^2 c_{U_i}(\mathbf{u}, \mathbf{v})\right), \end{aligned}$$

where $c_{Y_k}(\mathbf{u}, \mathbf{v}) = \text{Corr}[Y_k(\mathbf{u}), Y_k(\mathbf{v})]$ and $c_{U_i}(\mathbf{u}, \mathbf{v}) = \text{Corr}[U_i(\mathbf{u}), U_i(\mathbf{v})]$.

For $c_{Y_k}(\cdot)$ and $c_{U_i}(\cdot)$ we use exponential correlation functions, i.e. $c_{Y_k}(\mathbf{u}, \mathbf{v}) = \exp(-\|\mathbf{u} - \mathbf{v}\|/\xi_k)$ and $c_{U_i}(\mathbf{u}, \mathbf{v}) = \exp(-\|\mathbf{u} - \mathbf{v}\|/\phi_i)$ with correlation scale parameters ξ_k and ϕ_i . Other parametric correlation models might of course be used instead, depending on the application. Denote by $\boldsymbol{\theta}$ the concatenation of $\boldsymbol{\alpha}_k = (\alpha_{1k}, \dots, \alpha_{pk})^\top$, $k = 1, \dots, q$, $\boldsymbol{\xi} = (\xi_1, \dots, \xi_q)^\top$, $\boldsymbol{\sigma}^2 = (\sigma_1^2, \dots, \sigma_p^2)^\top$, and $\boldsymbol{\phi} = (\phi_1, \dots, \phi_p)^\top$. The cross PCF between X_i and X_j is then given by the parametric model:

$$g_{ij}(r; \boldsymbol{\theta}) = \exp\left(\sum_{k=1}^q \alpha_{ik}\alpha_{jk}\exp(-r/\xi_k) + 1[i=j]\sigma_i^2\exp(-r/\phi_i)\right). \quad (5)$$

If $\sum_{k=1}^q \alpha_{ik}\alpha_{jk}\exp(-r/\xi_k)$ is greater (smaller) than 0, this implies positive (negative) spatial correlation between points from X_i and X_j at the lag r . If for example $\alpha_{ik}\alpha_{jk} = 0$ for all $k = 1, \dots, q$, then X_i and X_j are independent.

The number q of latent common fields controls the complexity of the model and will be chosen according to a cross validation criterion detailed in Section 3.3. In Waagepetersen et al. (2016) and Choiruddin et al. (2019), estimation of $\boldsymbol{\theta}$ for a chosen q was based on a least squares criterion where non-parametric estimates of the pair correlation function acted as ‘dependent’ variables. These non-parametric estimates were based on fully specified regression models for the log intensity functions. This is not possible in our setting due to the presence of $\rho_0(\cdot)$. Section 3 therefore introduces a second order conditional composite likelihood function for estimation of $\boldsymbol{\theta}$ that does not require knowledge of $\rho_0(\cdot)$.

3. Second order conditional composite likelihood

We assume initially that the intensity function regression parameters $\boldsymbol{\beta}_i$ are known and thus suppress dependence on these in the notation. Recall also that $\boldsymbol{\theta}$ consists of the parameters for the PCFs and cross PCFs. The idea is to condition on the union of all points regardless of type and for each $\mathbf{u} \neq \mathbf{v} \in \cup_{i=1}^p X_i$ consider the conditional probability (see Section 1 in the supplementary material) that \mathbf{u} is of type i and \mathbf{v} is of type j :

$$p_{ij}(\mathbf{u}, \mathbf{v}; \boldsymbol{\theta}) = \frac{\rho_{ij}(\mathbf{u}, \mathbf{v})}{\sum_{k,l} \rho_{kl}(\mathbf{u}, \mathbf{v})} = \frac{f_i(\mathbf{u})f_j(\mathbf{v})g_{ij}(r; \boldsymbol{\theta}_{ij})}{\sum_{k,l} f_k(\mathbf{u})f_l(\mathbf{v})g_{kl}(r; \boldsymbol{\theta}_{kl})}, \quad (6)$$

where $f_i(\mathbf{u}) = \exp(\boldsymbol{\beta}_i^\top \mathbf{z}(\mathbf{u}))$, $i = 1, \dots, p$. Note that $\rho_0(\mathbf{u})\rho_0(\mathbf{v})$ cancels out in (6) so that the probabilities do not depend on the unspecified $\rho_0(\cdot)$. We then estimate $\boldsymbol{\theta}$ by maximizing the second order conditional composite likelihood function given by:

$$L(\boldsymbol{\theta}) = \prod_{i,j} \prod_{\substack{\mathbf{u} \in X_i \cap W, \mathbf{v} \in X_j \cap W \\ \mathbf{u} \neq \mathbf{v}}} 1_R[\mathbf{u}, \mathbf{v}] p_{ij}(\mathbf{u}, \mathbf{v}; \boldsymbol{\theta}), \quad (7)$$

where $1_R[\mathbf{u}, \mathbf{v}] = 1[\|\mathbf{u} - \mathbf{v}\| \leq R]$ and $R > 0$ is a user-specified tuning parameter. Specifying an $R < \infty$ is useful for reducing computing time. Moreover, omitting

pairs of points \mathbf{u} and \mathbf{v} that are distant from each other can improve statistical efficiency since such pairs do not provide much information on the correlation structure. As a rule of thumb, R should be chosen so that $g_{ij}(r; \boldsymbol{\theta}) \approx 1$ for $\|\mathbf{u} - \mathbf{v}\| > R$. Methods for choosing R are discussed in Lavancier et al. (2019).

The cross PCFs (5) and hence the second order conditional composite likelihood function are invariant to simultaneous interchange of columns $\boldsymbol{\alpha}_{\cdot k} = (\alpha_{ik})_k$ and corresponding correlation scale parameters ξ_k , as well as to multiplication by -1 of $\boldsymbol{\alpha}_{\cdot k}$. This lack of identifiability is not of much concern from a theoretical point of view since we are not interested in the individual α_{ij} 's but rather the resulting correlation structure which is invariant to the aforementioned transformations. From a practical point of view one might be worried about optimization convergence problems, e.g. the optimization algorithm (Section 3.1) jumping from one equivalent mode to another. However, in our simulation studies and data examples, for any particular set of initial values, the convergence to one particular equivalent mode was very stable.

Following the idea of two-step estimation in Waagepetersen and Guan (2009), we replace the parameters β_i by consistent estimates $\hat{\beta}_i$ obtained using the first order conditional composite likelihood (Hessellund et al., 2021) described in Section 2.2.

3.1. Optimization

We denote by $l_-(\boldsymbol{\theta})$ the negation of the log of (7) and turn the estimation of $\boldsymbol{\theta}$ into a minimization problem. In order to minimize $l_-(\boldsymbol{\theta})$ with respect to $\boldsymbol{\theta}$, we consider a cyclical block descent algorithm. The strategy is to update $\boldsymbol{\alpha}$, $\boldsymbol{\xi}$, $\boldsymbol{\sigma}^2$ and $\boldsymbol{\phi}$ in turn until a convergence criterion is met. In the following we will, with a convenient abuse of notation, use $\boldsymbol{\alpha}$ to denote both the matrix $[\alpha_{ij}]_{ij}$ and the vectorized version where the matrix is laid out column-wise $(\boldsymbol{\alpha}_1^\top, \dots, \boldsymbol{\alpha}_q^\top)^\top$. It will be clear from the context which interpretation of $\boldsymbol{\alpha}$ is relevant. Denote by $\boldsymbol{\theta}^{(n)} = ((\boldsymbol{\alpha}^{(n)})^\top, (\boldsymbol{\xi}^{(n)})^\top, (\boldsymbol{\sigma}^{2(n)})^\top, (\boldsymbol{\phi}^{(n)})^\top)^\top$ the current value of $\boldsymbol{\theta}$. We update each parameter using a quasi Newton-Raphson iteration with additional line search. This is equivalent to minimizing a certain least squares problem. We give the details of this since this is also needed for solving a regularized version of our estimation problem, see Section 3.2.

We denote by $\tilde{\boldsymbol{\theta}}$ a temporary parameter vector that keeps track of the updates leading from $\boldsymbol{\theta}^{(n)}$ to $\boldsymbol{\theta}^{(n+1)}$ and initialize $\tilde{\boldsymbol{\theta}} = \boldsymbol{\theta}^{(n)}$. Denote by $\tilde{\boldsymbol{\tau}} \in \{\tilde{\boldsymbol{\alpha}}, \tilde{\boldsymbol{\xi}}, \tilde{\boldsymbol{\sigma}}^2, \tilde{\boldsymbol{\phi}}\}$ the parameter vector to be updated and by $\tilde{\boldsymbol{\theta}}(\boldsymbol{\tau})$ the vector obtained by replacing $\tilde{\boldsymbol{\tau}}$ in $\tilde{\boldsymbol{\theta}}$ by $\boldsymbol{\tau}$. Consider a quadratic approximation of $l_-(\tilde{\boldsymbol{\theta}}(\boldsymbol{\tau}))$ with respect to $\boldsymbol{\tau}$ around $\tilde{\boldsymbol{\theta}}$:

$$q(\boldsymbol{\tau}) = l_-(\tilde{\boldsymbol{\theta}}) + (\boldsymbol{\tau} - \tilde{\boldsymbol{\tau}})^\top \mathbf{e}(\tilde{\boldsymbol{\tau}}) + \frac{1}{2}(\boldsymbol{\tau} - \tilde{\boldsymbol{\tau}})^\top \mathbf{H}(\tilde{\boldsymbol{\tau}})(\boldsymbol{\tau} - \tilde{\boldsymbol{\tau}}). \quad (8)$$

Here (omitting for convenience the arguments \mathbf{u}, \mathbf{v})

$$\mathbf{e}(\boldsymbol{\tau}) = \nabla_{\boldsymbol{\tau}} l_-(\tilde{\boldsymbol{\theta}}(\boldsymbol{\tau})) = \sum_{i,j} \sum_{\substack{\neq \\ \mathbf{u} \in X_i \cap W \\ \mathbf{v} \in X_j \cap W}} 1_R \left(\frac{\sum_{k,l} \nabla_{\boldsymbol{\tau}} \rho_{kl}(\tilde{\boldsymbol{\theta}}(\boldsymbol{\tau}))}{\sum_{k,l} \rho_{kl}(\tilde{\boldsymbol{\theta}}(\boldsymbol{\tau}))} - \frac{\nabla_{\boldsymbol{\tau}} \rho_{ij}(\tilde{\boldsymbol{\theta}}(\boldsymbol{\tau}))}{\rho_{ij}(\tilde{\boldsymbol{\theta}}(\boldsymbol{\tau}))} \right)$$

is the gradient with respect to $\boldsymbol{\tau}$ and

$$\mathbf{H}(\boldsymbol{\tau}) = \mathbb{E}[\nabla_{\boldsymbol{\tau}}^2 l_{-}(\tilde{\boldsymbol{\theta}}(\boldsymbol{\tau}))] = \int_{W^2} 1_R \text{Cov}\left(Z(\tilde{\boldsymbol{\theta}}(\boldsymbol{\tau}))\right) \sum_{i,j} \rho_{ij}(\tilde{\boldsymbol{\theta}}(\boldsymbol{\tau})) d\mathbf{u}d\mathbf{v}$$

is the expected Hessian with respect to $\boldsymbol{\tau}$. Here $Z(\mathbf{u}, \mathbf{v}, \tilde{\boldsymbol{\theta}}(\boldsymbol{\tau}))$ denotes a random vector which takes values $\nabla_{\boldsymbol{\tau}} \log(\rho_{ij}(\mathbf{u}, \mathbf{v}; \tilde{\boldsymbol{\theta}}(\boldsymbol{\tau})))$ with probabilities $p_{ij}(\mathbf{u}, \mathbf{v}; \tilde{\boldsymbol{\theta}}(\boldsymbol{\tau}))$ (Lemma 2.2 in the supplementary material). We estimate $\mathbf{H}(\tilde{\boldsymbol{\tau}})$ by

$$\hat{\mathbf{H}}(\tilde{\boldsymbol{\tau}}) = \sum_{i,j} \sum_{\substack{\neq \\ \mathbf{u} \in X_i \cap W, \mathbf{v} \in X_j \cap W}} 1_R[\mathbf{u}, \mathbf{v}] \text{Cov}\left(Z(\mathbf{u}, \mathbf{v}, \tilde{\boldsymbol{\theta}})\right),$$

which is unbiased by (2). Since $\hat{\mathbf{H}}(\tilde{\boldsymbol{\tau}})$ is a symmetric, positive semi-definite matrix, the eigendecomposition implies that $\hat{\mathbf{H}}(\tilde{\boldsymbol{\tau}})^{1/2} = U D^{1/2} U^T$, where D is the diagonal matrix of the (all non-negative) eigen values of $\hat{\mathbf{H}}(\tilde{\boldsymbol{\tau}})$ and U is the matrix of eigen vectors. Assuming that all the eigen values are positive, following Section 3 in the supplementary material, the minimizer $\hat{\boldsymbol{\tau}}$ of (8) is a solution of a least squares problem:

$$\hat{\boldsymbol{\tau}} = \arg \min_{\boldsymbol{\tau}} \left(\frac{1}{2} \|Y - X\boldsymbol{\tau}\|^2 \right) = (X^T X)^{-1} X^T Y, \quad (9)$$

where $Y = \hat{\mathbf{H}}(\tilde{\boldsymbol{\tau}})^{1/2} \left(-\hat{\mathbf{H}}(\tilde{\boldsymbol{\tau}})^{-1} \mathbf{e}(\tilde{\boldsymbol{\tau}}) + \tilde{\boldsymbol{\tau}} \right)$ and $X = \hat{\mathbf{H}}(\tilde{\boldsymbol{\tau}})^{1/2}$. Introducing a line search, we update $\boldsymbol{\tau}^{(n+1)} = \tilde{\boldsymbol{\tau}} + t(\hat{\boldsymbol{\tau}} - \tilde{\boldsymbol{\tau}})$, for some $t > 0$ and also update $\tilde{\boldsymbol{\theta}}$ by replacing $\tilde{\boldsymbol{\tau}} = \boldsymbol{\tau}^{(n)}$ by $\boldsymbol{\tau}^{(n+1)}$. When all components of $\tilde{\boldsymbol{\theta}}$ have been updated, we let $\boldsymbol{\theta}^{(n+1)} = \tilde{\boldsymbol{\theta}}$.

As mentioned in Section 2.3, we impose a sum to zero constraint on each $\boldsymbol{\alpha}_k$, i.e. $\sum_{i=1}^p \alpha_{ik} = 0$, $k = 1, \dots, q$. The constraint is easily accommodated by the change of variable $\mathbf{B}\boldsymbol{\psi} = \boldsymbol{\alpha}$, where $\boldsymbol{\psi}$ is a $(p-1) \times q$ matrix and $\mathbf{B}^T = [\mathbf{I}_{p-1} \ \mathbf{-1}]$ is a $(p-1) \times p$ matrix with \mathbf{I}_{p-1} the $(p-1) \times (p-1)$ identity matrix and $\mathbf{-1} = [-1, \dots, -1]^T \in \mathbb{R}^p$. Under the sum to zero constraint, the relation between $\boldsymbol{\alpha}$ and $\boldsymbol{\psi}$ is one-to-one. Thus in case of $\boldsymbol{\tau} = \boldsymbol{\alpha}$, we update the unconstrained parameter $\boldsymbol{\psi}$ using (by the chain rule) the gradient $\mathbf{B}^T \mathbf{e}(\tilde{\boldsymbol{\theta}})$ and the Hessian $\mathbf{B}^T \mathbf{H}(\tilde{\boldsymbol{\theta}}) \mathbf{B}$, and finally let $\boldsymbol{\alpha}^{(n+1)} = \mathbf{B}\boldsymbol{\psi}^{(n+1)}$.

The cyclical block updating is iterated until relative function convergence,

$$\left| \left[l_{-}(\boldsymbol{\theta}^{(n+1)}) - l_{-}(\boldsymbol{\theta}^{(n)}) \right] / l_{-}(\boldsymbol{\theta}^{(n)}) \right| < \epsilon, \quad (10)$$

for some $\epsilon > 0$ in which case we set $\hat{\boldsymbol{\theta}} = \boldsymbol{\theta}^{(n+1)}$. Algorithm 1 gives a brief overview of the cyclical block descent algorithm.

3.2. Optimization with lasso regularization

The overall model complexity is controlled by the number q of latent fields Y_j with associated parameters α_{ij} , $i = 1, \dots, p$, $j = 1, \dots, q$. Nevertheless, for any q , more sparse submodels could be obtained by restricting some α_{ij} to zero. Of course, if all

Algorithm 1 Cyclical block descent algorithm

- 1: Simulate initial parameters $\hat{\psi}^{(0)}$, $\hat{\xi}^{(0)}$, $\hat{\sigma}^{2(0)}$ and $\hat{\phi}^{(0)}$
 - 2: $n := 0$
 - 3: **repeat**
 - 4: $\tilde{\psi} := \psi^{(n)}$, $\tilde{\xi} := \xi^{(n)}$, $\tilde{\sigma}^2 := \sigma^{2(n)}$ and $\tilde{\phi} := \phi^{(n)}$
 - 5: update $\tilde{\psi}$, $\tilde{\xi}$, $\tilde{\sigma}^2$ and $\tilde{\phi}$ in turn using (9) combined with line search
 - 6: $\psi^{(n+1)} := \tilde{\psi}$, $\xi^{(n+1)} := \tilde{\xi}$, $\sigma^{2(n+1)} := \tilde{\sigma}^2$, $\phi^{(n+1)} := \tilde{\phi}$, and $\alpha^{(n+1)} := B\tilde{\psi}^{(n+1)}$
 - 7: $n := n + 1$
 - 8: **until** relative convergence criterion (10)
 - 9: **return** $\hat{\theta} = \theta^{(n)}$
-

entries in a column $\alpha_{\cdot k}$ are restricted to zero, this just corresponds to reducing q by one. In order to look for sparse submodels for a given q , we extend the estimation approach by introducing a lasso regularization on α . We express the sum to zero constraint for α by $C\alpha = \mathbf{0}$, where $C = [D_1 \cdots D_q]$ is a $q \times pq$ matrix that consists of submatrices D_i , $i = 1, \dots, q$, of dimension $q \times p$. Each submatrix D_i consists of ones on the i th row and zeros otherwise. Here α should be interpreted as the vector obtained by concatenating the $\alpha_{\cdot k}$, cf. Section 3.1. Note that the regularization is not relevant in the bivariate case $p = 2$ since in this case, by the sum to zero constraint, $\alpha_{1k} = 0$ implies $\alpha_{2k} = 0$ which just corresponds to reducing q by 1.

The regularized object function becomes:

$$l_-(\theta) + \lambda \sum_{i=1}^p \sum_{j=1}^q |\alpha_{ij}|, \quad C\alpha = \mathbf{0}, \quad (11)$$

where $\lambda \sum_{i=1}^p \sum_{j=1}^q |\alpha_{ij}|$ is a lasso penalty that can lead to exact zero components in the estimate of α . We minimize this using a cyclical block descent algorithm which only differs from the one in Section 3.1 by the update $\hat{\alpha} = \arg \min_{\alpha} \left(\frac{1}{2} \|Y - X\alpha\|^2 + \lambda \sum_{i=1}^p \sum_{j=1}^q |\alpha_{ij}| \right)$ subject to $C\alpha = \mathbf{0}$. To compute $\hat{\alpha}$ under the sum to zero constraint, we use the augmented Lagrangian algorithm suggested in Shi et al. (2016). Details are given in Section 4 in the supplementary material. In Section 3.3 we propose a cross validation procedure to choose λ .

The suggested algorithm can easily be extended to handle elastic net regularization (Zou and Hastie, 2005) that combines lasso with ridge regression. However, this introduces yet a tuning parameter controlling the convex combination of lasso and ridge regression. Also our main focus is sparsity as provided by the lasso. For simplicity of exposition, we therefore focus here on the lasso.

3.3. Determination of q and λ

We choose the values of q and λ according to a K -fold ($K \geq 2$) cross validation criterion constructed so that it targets selection of an appropriate cross correlation structure. Let for each i, j , M_{ij} denote the set of pairs (\mathbf{u}, \mathbf{v}) with $\mathbf{u} \in X_i$, $\mathbf{v} \in$

X_j , and $0 < \|\mathbf{u} - \mathbf{v}\| \leq R$. We randomly split M_{ij} into K equally sized subsets $M_{ij,1}, \dots, M_{ij,K}$. We then obtain for each $k = 1, \dots, K$, a parameter estimate $\hat{\boldsymbol{\theta}}_k$ by maximizing the regularized conditional composite likelihood

$$l_k(\boldsymbol{\theta}) = \sum_{i,j} \sum_{(\mathbf{u}, \mathbf{v}) \in M_{ij,-k}}^{\neq} \log p_{ij}(\mathbf{u}, \mathbf{v}; \boldsymbol{\theta}) + \lambda \sum_{i=1}^p \sum_{j=1}^q |\alpha_{ij}|, \quad \mathbf{C}\boldsymbol{\alpha} = \mathbf{0},$$

for the training data set consisting of the set of pairs $M_{ij,-k} = \cup_{l \neq k} M_{ij,l}$ where $M_{ij,k}$ is left out. The k th cross validation score based on the validation sets $M_{ij,k}$, $i \neq j$, is then

$$CV_k(q, \lambda) = \sum_{i \neq j} \sum_{(\mathbf{u}, \mathbf{v}) \in M_{ij,k}} \log p_{ij}(\mathbf{u}, \mathbf{v}; \hat{\boldsymbol{\theta}}_k).$$

We here omit the $M_{ii,k}$ to focus the cross validation on the fit of the cross correlation structure. To reduce the sensitivity to Monte Carlo variation, one may compute cross validation scores $CV_{kl}(q, \lambda)$, $l = 1, \dots, L$, based on L independent K -fold random splits of the data, and use the average $\overline{CV}(q, \lambda)$ of the $CV_{kl}(q, \lambda)$, $k = 1, \dots, K$, $l = 1, \dots, L$. We do not have a theoretical foundation for choosing K . We hence follow the rule of thumb in the statistical learning literature (Hastie et al., 2013) and choose K in the range of 5 to 10. Regarding L , a very large L can essentially eliminate the Monte Carlo variation due to the random splitting of the data into K folds. However, a moderate L is often used in practice to avoid excessive computing times. For example, we use $K = 5$ and $L = 10$ in our simulation studies in Section 4.

Consider the case $\lambda = 0$ which is relevant for example when $p = 2$. The most obvious choice of q is the one that minimizes the cross validation score, $q_{\min} = \arg \min_q \overline{CV}(q, 0)$. We denote this the minimum (MIN) rule. However, due to sensitivity to Monte Carlo error, a so-called one standard error rule has been proposed (Hastie et al., 2013) that promotes more sparse solutions. Let $SD(q, 0)$ denote the standard deviation of a cross validation score $CV_{kl}(q, 0)$ obtained from a single validation set. In the current framework, the one standard error (1-SE) rule selects the smallest q (denoted $q_{1\text{-SE}}$) for which $\overline{CV}(q, 0) \leq \overline{CV}(q_{\min}, 0) + SE(q_{\min}, 0)$, where $SE(q, 0) = SD(q_{\min}, 0) / \sqrt{KL}$ is the standard error of $\overline{CV}(q_{\min}, 0)$.

For joint selection of (q, λ) , the immediate choice would be the minimizer of $\overline{CV}(q, \lambda)$. However, computing $\overline{CV}(q, \lambda)$ over a two-dimensional grid of q and λ values is very time consuming. Instead we use a two-step approach where we first determine q_{\min} as in the previous paragraph and next choose the λ that minimizes $\overline{CV}(q_{\min}, \lambda)$ over values of λ . Thus the initial selection of q determines the overall model complexity while the subsequent possible selection of a $\lambda > 0$ may introduce additional sparsity given q_{\min} .

3.4. Model assessment

Assuming the model (3) for the intensity functions, Hessellund et al. (2021) obtained a consistent non-parametric estimate of any ratio $g_{ij}(r)/g_{lk}(r)$ of cross PCFs, $r > 0$, $i, j, l, k = 1, \dots, p$. Similarly, we can obtain semi-parametric estimates of these ratios

based on our semi-parametric estimates of the cross PCFs. If the assumed multivariate LGCP model is valid, the non-parametric and the semi-parametric estimates of cross PCF ratios should not differ much. In our data examples in Section 5 we informally assess the models by visual comparison of the two types of estimates. We also conduct a so-called global envelope goodness-of-fit test (Myllymäki et al., 2016) based on the difference between the two types of estimates over spatial lags $r \in [0, R]$. This requires simulation under a null model. For this we use the fitted multivariate LGCP where we replace the unknown background intensity ρ_0 by a non-parametric estimate introduced in Hessellund et al. (2021), see also Section 5 in the supplementary material. However, as discussed in Section 7, due to the impact of using an estimated ρ_0 it may be hard to interpret results of the model assessment - especially if a chosen summary statistic depends on the unknown ρ_0 .

4. Simulation study

In this section we use simulations to study the joint performance of the second order conditional composite likelihood, the optimization algorithm in Section 3.1 with additional lasso regularization in Section 3.2, and the cross validation procedure. We conduct simulation studies based on three different settings for a five-variate point process $\mathbf{X} = (X_1, X_2, X_3, X_4, X_5)^\top$ on $W = [0, 1]^2$. For the two first settings, \mathbf{X} is a multivariate LGCP. For the third setting, considered in Section 7 of the supplementary material, \mathbf{X} is a so-called product shot-noise Cox process. The construction of the random intensity function of a product shot-noise Cox process is very different from that of an LGCP. We consider the product shot noise Cox process to study how the proposed methodology works in case of a misspecified model. The qualitative conclusions from the third setting are quite similar to the first two settings. We therefore focus here on the details and results for the first two settings. Although it would be interesting to consider simulations from other types of multivariate models (e.g. Gibbs as in Rajala et al., 2018), we confine ourselves to multivariate models where the PCFs and cross PCFs are known.

For both LGCP settings we simulate one covariate $Z(\cdot)$ and one background intensity $\rho_0(\cdot) = 400 \exp(0.5V(\cdot) - 0.5^2/2)$, where Z and V are zero mean unit variance Gaussian random fields with exponential and Gaussian correlation functions, i.e. $\text{Corr}(Z(\mathbf{u}), Z(\mathbf{v})) = \exp(-\|\mathbf{u} - \mathbf{v}\|/0.05)$ and $\text{Corr}(V(\mathbf{u}), V(\mathbf{v})) = \exp(-(\|\mathbf{u} - \mathbf{v}\|/0.2)^2)$. The particular realizations of Z and ρ_0 are shown in Figure 1. These realizations are fixed throughout the simulation study.

Table 1 shows the values used for the intensity function regression parameters γ , and the standard deviation and correlation scale parameters σ and ϕ for the type-specific latent fields. The table also shows the expected number of points N for each point process. Regarding the number q of common latent fields with associated coefficients α and correlation scale parameters ξ , we take $q = 0$ for the first setting resulting in a case with independent components X_1, \dots, X_5 . In the second setting we let $q = 2$ and choose α as specified in the table left in Figure 2. We moreover let $\xi_1 = 0.02$ and $\xi_2 = 0.03$. The resulting PCFs and cross PCFs are shown in the middle and right plots in Figure 2. In the case $q = 2$ we have a positive spatial

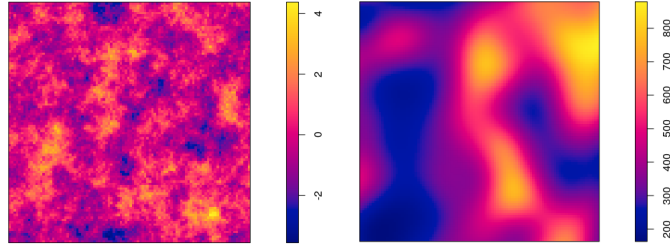


Fig. 1. Left: simulated covariate Z . Right: simulated ρ_0 .

Table 1. Simulation settings for X in each setup $q = 0, 2$ (excluding α and ξ).

| X | γ_1 | γ_2 | σ | ϕ | N | X | γ_1 | γ_2 | σ | ϕ | N |
|-------|------------|------------|----------|--------|-----|-------|------------|------------|----------|--------|-----|
| X_1 | 0.1 | -0.1 | 0.71 | 0.02 | 550 | X_4 | 0.4 | 0.1 | 0.71 | 0.03 | 750 |
| X_2 | 0.2 | -0.2 | 0.71 | 0.02 | 619 | X_5 | 0.5 | 0.2 | 0.71 | 0.04 | 830 |
| X_3 | 0.3 | 0 | 0.71 | 0.03 | 677 | | | | | | |

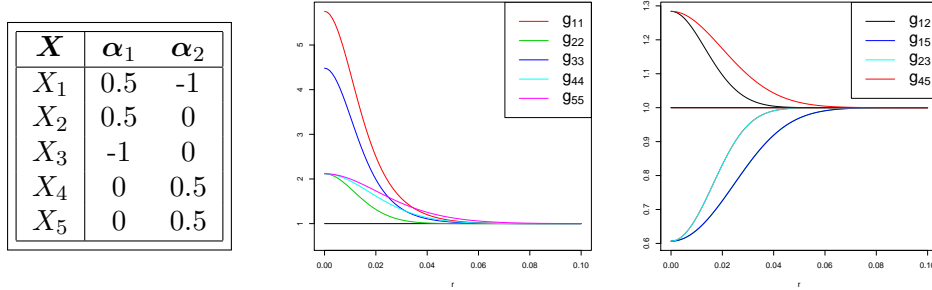


Fig. 2. Left: α . Middle: true PCFs. Right: true cross PCFs (note $g_{13} = g_{23}$ and $g_{14} = g_{15}$).

dependence between X_1 and X_2 and between X_4 and X_5 , while there is a negative spatial dependence between X_3 and (X_1, X_2) and between X_1 and (X_4, X_5) .

For our second order conditional composite likelihood we specified exponential correlation models for the fields Y_k , $k = 1, \dots, q$ and U_i , $i = 1, \dots, 5$. In practice it is rarely the case that the true correlation models correspond exactly to the specified ones. To reflect this we simulate the Y_k and U_i using Gaussian correlation functions, i.e. $\text{Corr}(Y_k(\mathbf{u}), Y_k(\mathbf{v})) = \exp(-(\|\mathbf{u} - \mathbf{v}\|/\xi_k)^2)$ and $\text{Corr}(U_i(\mathbf{u}), U_i(\mathbf{v})) = \exp(-(\|\mathbf{u} - \mathbf{v}\|/\phi_i)^2)$. Hence the model applied is misspecified for the simulated data. For each setting we generate 100 simulated realizations of \mathbf{X} .

In both settings we select q among the values $0, 1, \dots, 5$, and next, for the chosen q , λ among the values $10, 8, 6, 5, 4, 3, 2, 1, 0.5, 0.25, 0$. For this we use cross validation with $K = 5$ and $L = 10$. We consider results using both the MIN and the 1-SE approach for the selection of q . To assess the effect of regularization in an overparametrized setting, we also report results where $q = 7$ is fixed with λ chosen by cross validation. For the second order conditional composite likelihood we only

consider distinct pairs of points \mathbf{u}, \mathbf{v} with $\|\mathbf{u} - \mathbf{v}\| \leq R = 0.1$. The initial values for the components of $\boldsymbol{\theta} = (\boldsymbol{\alpha}, \boldsymbol{\xi}, \boldsymbol{\sigma}^2, \boldsymbol{\phi})$ are simulated as $\alpha_{ik} \sim \text{Unif}(-0.25, 0.25)$, $\xi_k, \phi_i \sim \text{Unif}(0.01, 0.04)$ and $\sigma_i^2 \sim \text{Unif}(0.4, 0.6)$. The parameter ϵ in the relative function convergence criterion (10) is set to 10^{-5} and the convergence parameters $\tilde{\epsilon}$ and $\tilde{\tau}$ for the regularized optimization ((3) in the supplementary material) are set to 10^{-10} .

We measure the performance for each selected model using mean integrated squared error (MISE) aggregated over respectively all PCFs and all cross PCFs, i.e.

$$\text{MISE}_{\text{between}}(\hat{\boldsymbol{\theta}}) = \sum_{i < j} \text{E} \left[\int_{0.01}^{0.1} \left(g_{ij}(r; \hat{\boldsymbol{\theta}}_{ij}) - g_{ij}(r; \boldsymbol{\theta}_{ij}) \right)^2 dr \right]. \quad (12)$$

We also consider $\text{MISE}_{\text{within}}(\hat{\boldsymbol{\theta}})$ and $\text{MISE}_{\text{total}}(\hat{\boldsymbol{\theta}})$ defined as $\text{MISE}_{\text{between}}(\hat{\boldsymbol{\theta}})$ but with sum over $i = j$ or $i \leq j$.

We compare the performance of the proposed method with two non-parametric approaches. For the first approach, referred to as ‘simple’, we estimate the intensity functions non-parametrically using the `spatstat` (Baddeley et al., 2015) procedure `density.ppp` with bandwidths selected using the method introduced in Cronie and van Lieshout (2018). Next the PCFs and cross PCFs are estimated using the `spatstat` procedures `pcfinhom` and `crosspcfinhom` with the intensity functions replaced by the non-parametric estimates. For the PCF and cross PCF estimation we manually specify reasonable bandwidths based on the knowledge of the true PCFs and cross PCFs (note that this is in favor of the non-parametric approach). The second approach, referred to as ‘Diggle’, is an adaption to the multivariate case of the method proposed in Diggle et al. (2007) (see Section 6 in the supplementary material for details). To measure the performances of the non-parametric approaches we simply replace the fitted parametric cross PCFs in (12) by the non-parametric estimates.

4.1. Five-variate LGCP with zero common latent fields

In the case $q = 0$, the MIN rule only selects the true value $q = 0$ for 1% of the simulated data sets while values of $q = 1, 2, 3$ are selected for 99% of the simulations, see left Table 2. Using the 1-SE rule, $q = 0$ is selected in 77% of the cases and a value of q bigger than 1 is only selected in two cases. The reason that the MIN rule frequently selects q larger than zero may be that neither of the models with $q = 0, \dots, 3$ are severely overparametrized. E.g. with $q = 3$, the in total 15 PCFs and cross PCFs are parametrized using just 25 parameters, i.e. less than 2 parameters on average for each PCF or cross PCF. Hence overfitting that can be detected by the cross validation procedure mainly occurs for $q = 4, 5$. The middle third column in Table 2 (left) shows 95% probability intervals for the selected λ s when $q = 1, 2, 3$ and the last column shows the average percentages of α_{ik} ’s that are estimated to be 0. These columns show that when a larger q is selected, then also a larger λ is selected leading to a higher percentage of zeros in the estimated $\boldsymbol{\alpha}$. This makes sense since larger q means more superfluous parameters and hence more need for

Table 2. (Left: true $q = 0$. Right: true $q = 2$) Distribution of q chosen by MIN and 1-SE rules, 95% probability interval for selected λ s, and averages over simulated data sets of percentages of estimated α_{ik} s equal to zero.

| q | MIN | 1-SE | λ | (% $\alpha_{ik} = 0$) | MIN | 1-SE | λ | (% $\alpha_{ik} = 0$) |
|-----|-----|------|-----------|------------------------|-----|------|-----------|------------------------|
| 0 | 1 | 77 | - | - | 0 | 0 | - | - |
| 1 | 32 | 21 | (0;0.61) | 2 | 2 | 39 | 0 | 0 |
| 2 | 56 | 2 | (0;0.41) | 7 | 60 | 61 | (0;0.38) | 1 |
| 3 | 11 | 0 | (0;0.88) | 6 | 36 | 0 | (0;0.25) | 0.6 |
| 4 | 0 | 0 | - | - | 2 | 0 | 0 | 0 |
| 7 | - | - | (0;4.52) | 52 | - | - | (0;2) | 26 |

regularization. In the case $q = 7$, the selected λ s tend to be markedly larger than for the smaller q s up to 3. Also 52% of the α_{ik} are estimated to be zero in the case $q = 7$ while the percentages are quite small for q up to 3. For $q = 1, 2, 3$, the selected λ was zero (meaning no regularization) in 59%, 57%, and 55% of the cases indicating that $q = 1, 2, 3$ already leads to a rather sparse setup and explaining the small percentages of α_{ik} estimated to be zero. Figure 3 shows the average of $\overline{CV}(q, 0)$ over all simulated data sets and confirms that the CV scores are quite similar across different q .

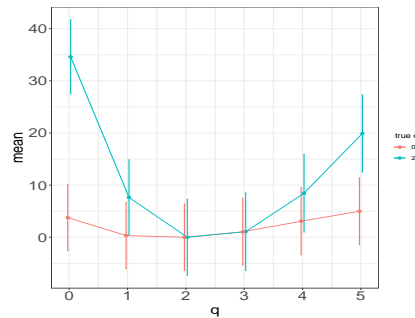
**Fig. 3.** Averages over simulated data sets of $\overline{CV}(q, 0)$ scores with minimum average CV-score subtracted. The bars show the average of the standard errors $SE(q, 0)$ obtained for $\overline{CV}(q, 0)$ for each simulated data set. Red is for $q = 0$ while blue is for $q = 2$.

Figure 4 shows means and 95% pointwise probability intervals for estimates of a subset of the PCFs and cross PCFs obtained for the simulated data sets with q selected among 0, 1, 2, 3, 4, 5 using either MIN or 1-SE and with $\lambda = 0$. We only show estimates with no regularization since the regularized estimates are very similar. The means are quite similar for MIN and 1-SE, and the MIN and 1-SE estimates are close to unbiased for the cross PCFs. A moderate bias is present for the PCF. This is not unexpected as we specify the wrong parametric model. However, the simple non-parametric estimates are strongly biased in all cases.

Table 3 gives total, within, and between MISEs with different strategies for choosing (q, λ) and for the two non-parametric approaches. The non-parametric approaches are clearly outperformed by the semi-parametric method. The results

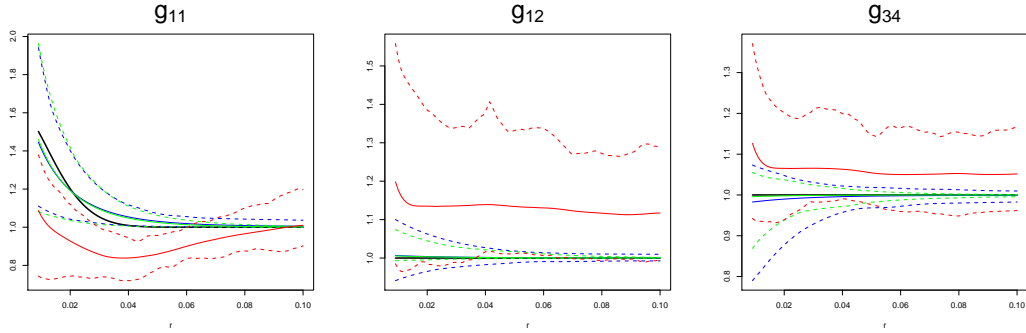


Fig. 4. (true $q = 0$) Blue, green and red solid lines indicate pointwise means of estimates for selected cross PCFs using MIN, 1-SE, or simple non-parametric estimation. The dotted lines indicate the corresponding 95% pointwise probability intervals. Black solid lines indicate true cross PCFs.

Table 3. MISE using $(q_{\min}, 0)$, (q_{\min}, λ) , $(q_{1-SE}, 0)$, simple, or Diggle's non-parametric approach when true $q = 0$.

| | $(q_{\min}, 0)$ | (q_{\min}, λ) | $(q_{1-SE}, 0)$ | simple | Diggle |
|-------------------------|----------------------|-----------------------|----------------------|----------------------|----------------------|
| $MISE_{\text{total}}$ | $3.77 \cdot 10^{-4}$ | $3.78 \cdot 10^{-4}$ | $3.81 \cdot 10^{-4}$ | $2.22 \cdot 10^{-3}$ | $2.63 \cdot 10^{-3}$ |
| $MISE_{\text{within}}$ | $1.02 \cdot 10^{-3}$ | $1.02 \cdot 10^{-3}$ | $1.11 \cdot 10^{-3}$ | $4.58 \cdot 10^{-3}$ | $3.36 \cdot 10^{-3}$ |
| $MISE_{\text{between}}$ | $5.45 \cdot 10^{-5}$ | $5.34 \cdot 10^{-5}$ | $2.01 \cdot 10^{-5}$ | $1.04 \cdot 10^{-3}$ | $2.27 \cdot 10^{-3}$ |

for MIN with $\lambda = 0$ or λ selected are very similar and also similar to 1-SE in case of $MISE_{\text{within}}$. However, $MISE_{\text{between}}$ for cross PCFs is more than twice as big for MIN compared to 1-SE. This is not so surprising since 1-SE chooses the true $q = 0$ most of the time while MIN tends to choose larger values of q . The between MISEs are on the other hand on a much smaller scale than the within MISEs.

4.2. Five-variate LGCP with two common latent fields

In case of $q = 2$, both MIN and 1-SE performs quite well in the sense that the chosen q 's differ at most by one from the true q in 98% (MIN) or in 100% (1-SE) of the cases and the true $q = 2$ is chosen in 60% (MIN) or 61% (1-SE) of the cases. The λ column in Table 2 (right) shows 95% probability intervals for the selected λ s. For $q = 1, 4$ the cross validation always selected $\lambda = 0$. The selected λ s for $q = 2, 3$ are in general small and 80% ($q = 2$) or 95% ($q = 3$) of the λ s were selected to be zero. These results indicate that regularization is not pertinent in this case where the true α is not particularly sparse. Also the percentages of α_{ik} estimated to be zero are very small for $q = 1, 2, 3, 4$. In case of the overparametrized model $q = 7$ we on the other hand do see an effect of regularization with larger selected λ s, and on average 26% of the α_{ik} s estimated to be zero.

Figure 5 shows means and 95% probability intervals for selected estimated PCFs and cross PCFs obtained with MIN or 1-SE without regularization. In both cases MIN and 1-SE produce some bias for the PCFs, which is expected as we specify the

Table 4. MISE using $(q_{\min}, 0)$, (q_{\min}, λ) , $(q_{1\text{-SE}}, 0)$, the simple or Diggle non-parametric approach when true $q = 2$.

| | $(q_{\min}, 0)$ | (q_{\min}, λ) | $(q_{1\text{-SE}}, 0)$ | simple | Diggle |
|--------------------------------|----------------------|-----------------------|------------------------|----------------------|----------------------|
| $\text{MISE}_{\text{total}}$ | $1.64 \cdot 10^{-3}$ | $1.64 \cdot 10^{-3}$ | $1.65 \cdot 10^{-3}$ | $7.25 \cdot 10^{-3}$ | $4.91 \cdot 10^{-3}$ |
| $\text{MISE}_{\text{within}}$ | $4.43 \cdot 10^{-3}$ | $4.42 \cdot 10^{-3}$ | $4.40 \cdot 10^{-3}$ | $2.04 \cdot 10^{-2}$ | $8.63 \cdot 10^{-3}$ |
| $\text{MISE}_{\text{between}}$ | $2.43 \cdot 10^{-4}$ | $2.43 \cdot 10^{-4}$ | $2.71 \cdot 10^{-4}$ | $6.76 \cdot 10^{-4}$ | $3.05 \cdot 10^{-3}$ |

wrong model. As in the case $q = 0$, the non-parametric estimates are more biased than the semi-parametric estimates.

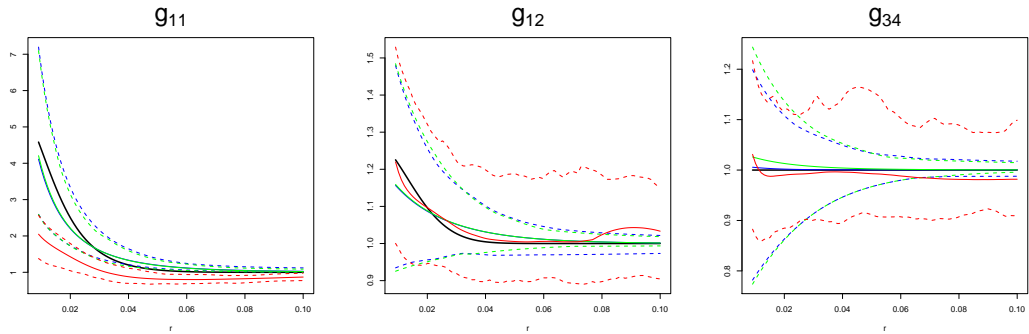


Fig. 5. (true $q = 2$) Blue, green and red solid lines indicate pointwise means of estimates for selected cross PCFs using MIN, 1-SE, or simple non-parametric estimation. The dotted lines indicate the corresponding 95% pointwise probability intervals. Black solid lines indicate true cross PCFs.

Table 4 shows that MIN and 1-SE perform very similar regarding MISE. In case of $\text{MISE}_{\text{between}}$, MIN and 1-SE are somewhat better than the simple approach but much better than Diggle’s approach. On the other hand, MIN and 1-SE are somewhat better than Diggle’s approach but much better than the simple approach in terms of $\text{MISE}_{\text{within}}$. Overall ($\text{MISE}_{\text{total}}$) the semi-parametric method outperforms the non-parametric methods.

5. Data examples

In the following we apply our new methodology to point patterns of cells in tumor tissue and crime scenes in Washington DC. We remind that the parameter matrix α consists of coefficients for the common latent fields, σ is the vector of standard deviations for the type-specific latent fields, and ξ and ϕ are vectors of correlation scale parameters for the common and type-specific latent fields.

5.1. Lymph node metastasis

Cancer malignancies are complex tissues containing many different cell types that may have opposing roles in tumor growth (Valkenburg et al., 2018). It is now recognized that the interactions between the multiple cell types determine the intrinsic

aggressiveness of a tumor and its response to a given anti-cancer treatment. Studying each cell type separately is therefore inadequate (Weinberg, 2014; Tsujikawa et al., 2017). With modern multiplexing technology it is now possible to image a large number of cell types simultaneously. Figure 6 (left) is a specific example, which shows a fluorescence image of a lymph node metastasis. Figure 6 also shows point patterns of locations of four types of cells extracted from the image using machine learning techniques. The four types of cells (with abbreviated names and numbers

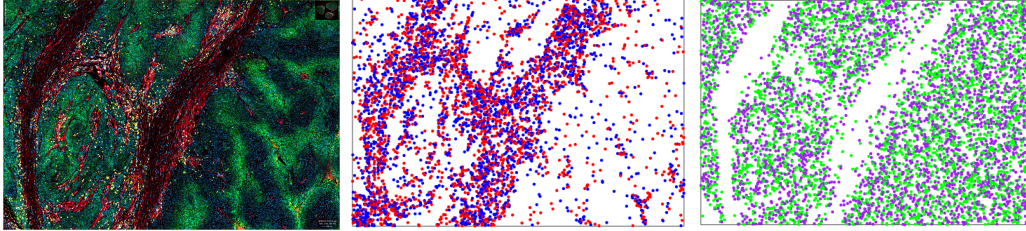


Fig. 6. Left: fluorescence image of a lymph node metastasis. Middle: bivariate point pattern of CD8 (blue) and 50% independently thinned Stroma (red) cells. Right: bivariate point pattern of 80% independently thinned Hypoxic (purple) and 80% independently thinned Normoxic (green) cells (data kindly provided by Arnulf Mayer, Dept. of Radiation Oncology, University Medical Center, Mainz, Germany).

of cells in parantheses) are Hypoxic tumor cells (Hypoxic, 11733), Normoxic tumor cells (Normoxic, 18469), Stroma cells (Stroma, 6015), and Cytotoxic T-lymphocytes (CD8, 1466). For better visualization we only show random subsets obtained by independent thinnings of the points. Our aim is to characterize the point patterns in terms of their intensity functions and their PCFs and cross PCFs. We thereby quantify trends and within/between interactions for the different types of cells. Such characterizations may be used in subsequent studies e.g. for predicting outcomes of cancer treatments (see for example Herbst et al., 2014; Yan et al., 2019).

Figure 7 shows non-parametric estimates of the intensity functions for the four point patterns. These plots show a strong segregation between the patterns of Stroma and CD8 cells versus the tumor cells. In the following we study the more subtle variation within the bivariate point patterns of Stroma and CD8 respectively Normoxic and Hypoxic.

There are no spatial covariates available for this data set. The intensity functions are therefore proportional to the common component $\rho_0(\cdot)$ both for the pairs Stroma,CD8 and Normoxic,Hypoxic. Since the point patterns are of high cardinality we reduce computing time by working with independent thinnings of the point patterns. The PCFs and cross PCFs are invariant to independent thinning while the intensity functions are only changed by a multiplication with the thinning probability. In the following we present a detailed analysis of the Stroma-CD8 point pattern. The analysis for the Normoxic-Hypoxic tumor cells is quite similar and is presented in Section 8 of the supplementary material.

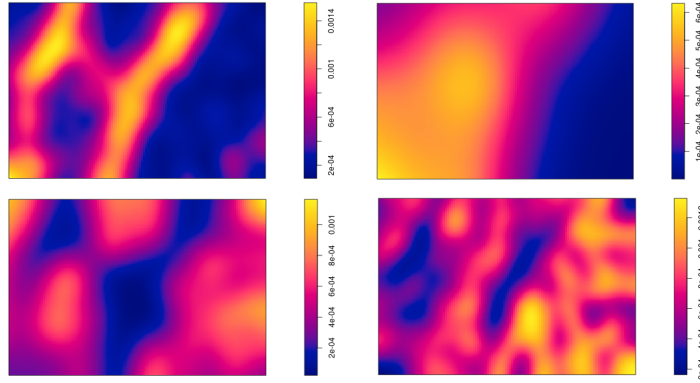


Fig. 7. Kernel estimates of the intensity functions for Stroma (upper left), CD8 (upper right), Hypoxic (lower left) and Normoxic (lower right) with bandwidths 121.2, 359.5, 173.9 and 115.7, respectively.

5.1.1. *Stroma and CD8*

For Stroma and CD8 we use all CD8 points and independently thin the Stroma points with a thinning probability of 50%. The point patterns clearly show some large scale trends (Figure 7) that are not easily fitted by simple parametric models. We instead assume the model (3), choose CD8 as the baseline, and following Hessellund et al. (2021) estimate $\beta = (\beta_{\text{Str}}, \beta_{\text{CD8}})^T = (\gamma_{\text{Str}} - \gamma_{\text{CD8}}, \gamma_{\text{CD8}} - \gamma_{\text{CD8}})^T$ by $\hat{\beta}_{\text{Str}} = \log(3007/1466) = 0.72$ and $\hat{\beta}_{\text{CD8}} = 0$. We next choose q among the values $\{0, 1, 2\}$ using a 5-fold cross validation as described in Section 3.3, where we resample $L = 10$ times. We choose the maximal interpoint distance R for pairs of points to be $400 \mu\text{m}$ which corresponds to approximately 15% of the largest observation window side length. According to the left panel in Figure 8 we choose $q = 1$

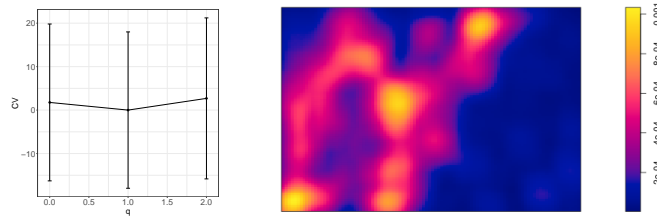


Fig. 8. Left: CV-scores (minus minimum CV-score) with standard errors. Right: non-parametric estimate of ρ_0 with bandwidth = 194.5.

that minimizes the cross validation score. The right panel in Figure 8 shows a non-parametric estimate of ρ_0 using the estimator introduced in Hessellund et al. (2021) with bandwidth chosen as described in Section 5 in the supplementary material.

According to the parameter estimates in Table 5 and the resulting PCFs and cross PCFs shown in the left panel of Figure 9, both Stroma and CD8 are randomly clustered point processes. The clustering is partly negatively correlated (cf. $\hat{\alpha}$ and the fitted cross PCF in Figure 9) and partly independent (cf. $\hat{\sigma}$) between Stroma

Table 5. Parameter estimates for Stroma and CD8 for $q = 1$.

| | $\hat{\alpha}$ | $\hat{\xi}$ | $\hat{\sigma}$ | $\hat{\phi}$ | | $\hat{\alpha}$ | $\hat{\xi}$ | $\hat{\sigma}$ | $\hat{\phi}$ |
|--------|----------------|-------------|----------------|--------------|-----|----------------|-------------|----------------|--------------|
| Stroma | 0.52 | 63.4 | 0.32 | 97.7 | CD8 | -0.52 | 63.4 | 0.78 | 193.6 |

and CD8. The strongest clustering is found for CD8 due to the higher value of $\hat{\sigma}_{CD8}$ than $\hat{\sigma}_{Str}$, see also the fitted PCFs in Figure 9.

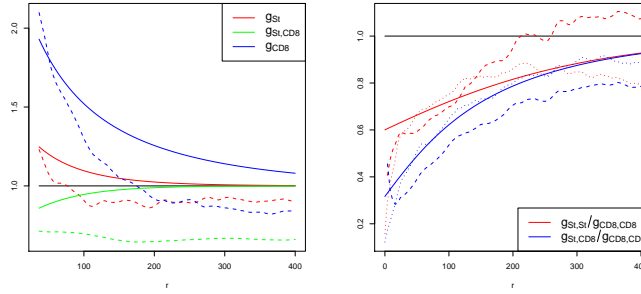


Fig. 9. Left: estimated (cross) PCFs using the semi-parametric model (solid) and simple approach (dashed). Right: estimated (cross) PCF ratio using semi-parametric model (solid), simple approach (dashed) and consistent approach (dotted).

The total estimated variances for the log random intensity functions of Stroma and CD8 are rather moderate, respectively 0.37 and 0.88, while the empirical variance of $\log \hat{\rho}_0$ over the observation window is 1.15. In this sense, the majority of the variation in the random intensity functions (especially for Stroma) is explained by ρ_0 .

Following Section 3.4, the right panel in Figure 9 compares semi-parametric estimates of cross PCF ratios g_{Str}/g_{CD8} and $g_{Str,CD8}/g_{CD8}$ with the non-parametric estimates introduced in Hessellund et al. (2021). The agreement seems reasonable and this is confirmed by global envelope p -values of 0.05 in case of g_{Str}/g_{CD8} and 0.09 for $g_{Str,CD8}/g_{CD8,CD8}$, see also the global envelope plots in Section 9 in the supplementary material. Section 11 in the supplementary material further comments on model assessment using the inhomogeneous cross J -function (Cronie and van Lieshout, 2016).

Figure 9 (left) also shows simple non-parametric PCF and cross PCF estimates which are generally smaller than the semi-parametric estimates. In particular, the non-parametric estimate of the cross PCF suggests a strong negative correlation between Stroma and CD8 for all spatial lags considered. As discussed in Shaw et al. (2020), this might be due to that the selected bandwidths imply too little smoothing in the non-parametric intensity estimates (upper plots in Figure 7). Figure 9 (right) further shows that the simple estimates of cross PCF ratios deviate more from the consistent non-parametric estimates than the semi-parametric estimates.

5.2. Washington DC street crimes

It is of great interest for criminologists and police authorities to study the spatial patterns of crime scenes since this can lead to better understanding of factors affecting crime and more efficient policing strategies. There are several competing theories regarding how crime occurrence depends on environmental factors (Weisburd et al., 1993; Haberman, 2017). Such theories may be studied using the intensity model (3). Next, estimates of PCFs and cross PCFs (5) may be used to assess whether crime occurrence is fully explained by the available covariates through the intensity function. If estimated PCFs and cross PCFs differ markedly from one, this is a sign of unexplained random variation that may call for further criminological investigation. Further, if cross correlations exist between different crimes, this means that predictions of one type of crime may be enhanced by consideration of other types of crimes.

In this section, we focus on the spatial correlation between six common types of street crimes committed in Washington DC in January and February 2017. The

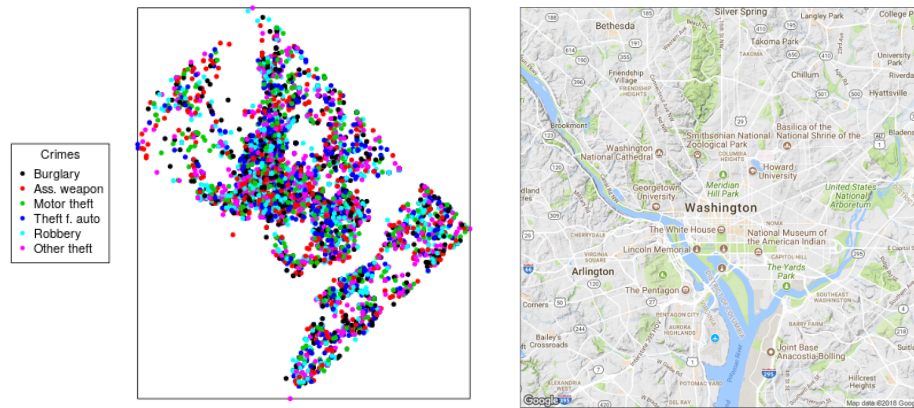


Fig. 10. Left: street crimes locations ($n = 5378$). Right: a map of Washington DC. The data set is extracted from a larger data set publicly available from <http://opendata.dc.gov/datasets/>.

six types of crimes with numbers in parantheses are 1) Burglary (259), 2) Assault with weapon (332), 3) Motor vehicle theft (335), 4) Theft from automobile (1832), 5) Robbery (366), and 6) Other theft (2254). The locations of the six types of crimes are illustrated in Figure 10. This data set has previously been considered by Hessellund et al. (2021) who focused on the dependency of the street crime intensity functions on spatial covariates using the model (3). In the following we focus on the second order properties as described by the PCFs and cross PCFs. We refer to Hessellund et al. (2021) for more details regarding the covariates and the fitted intensity functions.

We apply the regularized estimation approach described in Sections 3.2-3.3 where we first determine q using cross validation without regularization and next, for the chosen q , use another cross validation to select the regularization parameter λ to potentially obtain a sparse submodel for the chosen q . For the cross

validation, we use $K = 5$ and $L = 10$, and choose q in $\{0, 1, \dots, 5\}$ and λ in $\{100, 80, 60, 50, 40, 30, 20, 10, 5, 2.5, 1, 0.25, 0\}$. For the second order composite likelihood we use $R = 1000$ meters.

The left panel in Figure 11 shows cross validation scores for each q , where the 1-SE criterion leads to choosing $q = 0$ while MIN chooses $q = 1$. The middle panel shows CV-scores for each λ with $q = 1$, where the minimum is obtained for $\lambda = 0$. The right panel in Figure 11 shows a non-parametric estimate of ρ_0 using the estimator described in Hessellund et al. (2021) with bandwidth chosen as described in Section 3.3 in the supplementary material. This is our current best proposal for a data-driven estimate of ρ_0 . It may, however, seem too smooth since ρ_0 is supposed to capture complex variation in the intensity due to urban structure and varying population density. In the following we focus on the results with $q = 1$ and $\lambda = 0$. Hence we obtain an estimate of α without regularization.

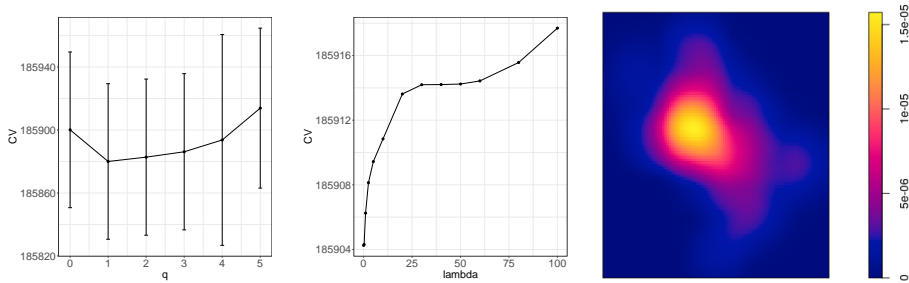


Fig. 11. Left: CV-score for q with one standard error bars. Middle: CV-score for λ given $q = 1$. Right: non-parametric estimate of ρ_0 with bandwidth 2654 meters.

The parameter estimates for each street crime are given in Table 6 except for the common latent field correlation scale parameter estimate which is $\hat{\xi} = 102.5$. The σ_i estimates are small to moderate for the first five crimes while the estimate $\hat{\sigma}_6$ for Other theft is about two times larger than the other σ_i estimates. Regarding the latent field Y_1 , the α_{i1} estimates are pretty small for Assault, Vehicle theft, Theft from auto, and Robbery while α_{11} for Burglary and α_{61} for Other theft have fairly large estimates 0.78 and -0.93 . The resulting estimated PCFs and cross PCFs are shown in the left and middle panels of Figure 12. The overall conclusion is that most crimes are moderately clustered except for Burglary and Other theft with strongest clustering for Other theft. Also the cross dependencies seem fairly weak except for the pairs Burglary and Vehicle (crimes 1 and 3, positively correlated) and Burglary and Other theft (crimes 1 and 6, negatively correlated). The interpretation of these results is that except for moderate random fluctuations, the spatial patterns of Assault, Vehicle theft, Theft from auto and Robbery are quite well described by their intensity functions depending on the common factor ρ_0 as well as covariate effects. On the other hand, the random intensity functions for Burglary and Other theft seem subject to more pronounced deviations from the intensity functions, and these deviations are negatively correlated. In other words, if a cluster of Burglaries not explained by the intensity function is present in a certain area, then there tends

Table 6. Table of parameter estimates for each street crime for $(q, \lambda) = (1, 0)$. Last two columns show estimates of α_l , $l = 1, 2$ with $(q, \lambda) = (2, 2.5)$.

| Crime type | $\hat{\alpha}$ | $\hat{\sigma}$ | $\hat{\phi}$ | $\hat{\alpha}_{.1}$ | $\hat{\alpha}_{.2}$ |
|---------------|----------------|----------------|--------------|---------------------|---------------------|
| Burglary | 0.78 | 0.50 | 245.8 | 0 | 0.76 |
| Assault | -0.12 | 0.51 | 457.5 | 0 | -0.09 |
| Vehicle Theft | 0.49 | 0.14 | 20.5 | 0 | 0.47 |
| Theft F. Auto | 0.09 | 0.58 | 2483.1 | 0 | 0.08 |
| Robbery | -0.30 | 0.53 | 485.2 | 0 | -0.26 |
| Other theft | -0.93 | 0.96 | 20.5 | 0 | -0.97 |

to be less Other theft committed in the same area and vice versa.

We also tried out $q = 2$ for which the cross validation score is quite close to the one for $q = 1$. For $q = 2$ the cross validation selected $\lambda = 2.5$. The last columns in Table 6 show the estimate of α obtained with $(q, \lambda) = (2, 2.5)$. The lasso regularization has shrunk $\hat{\alpha}_{.1}$ to $\mathbf{0}$, while the estimate of $\alpha_{.2}$ is quite similar to the estimate of $\alpha_{.1}$ for $q = 1$. In view of this, one may argue that the lasso regularization makes our estimation approach more robust, since a too large selected q can be counterbalanced by regularization on α with a $\lambda > 0$.

Quite different conclusions are obtained with the simple non-parametric analysis. Figure 12 shows that the non-parametric estimates of the PCFs and cross PCFs are all considerably above the reference value one, which would imply strong clustering within and between the different types of crime. These results may well be explained by bias of the non-parametric estimates.

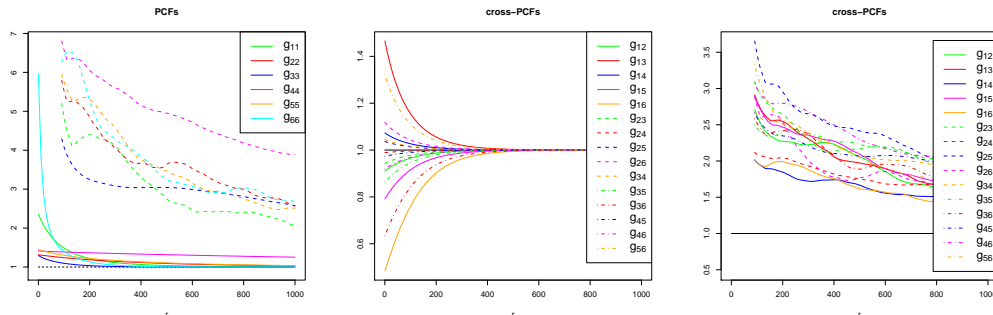


Fig. 12. Left: semi-parametric (solid) and simple non-parametric (dashed) estimates of PCFs for $(q, \lambda) = (1, 0)$. Middle: semi-parametric estimates of cross PCFs for $(q, \lambda) = (1, 0)$. Right: simple non-parametric estimates of cross PCFs.

For model assessment, we consider global envelope tests based on differences between semi-parametric and consistent non-parametric estimates for all 20 ratios g_{ij}/g_{66} , $1 \leq i \leq j \leq 6$, $(i, j) \neq (6, 6)$. The p -values obtained are between 0.089 and 0.624, and hence do not provide evidence against our model. Some representative global envelope plots for the differences are shown in Section 10 in the supplementary material. Further model assessment using the inhomogeneous cross J -function is

discussed in Section 11 in the supplementary material.

We finally consider an explorative analysis focusing on patterns in the common latent process Y_1 . We define ‘residuals’ $\Delta \log \Lambda_i(\mathbf{u})$ by $\log \Lambda_i(\mathbf{u}) - \mu_i - \beta_i^\top \mathbf{z}(\mathbf{u}) - \frac{1}{p} \sum_{l=1}^p [\log \Lambda_l(\mathbf{u}) - \mu_l - \beta_l^\top \mathbf{z}(\mathbf{u})]$. Due to the sum-to-zero constraint on α we obtain $\Delta \log \Lambda_i(\mathbf{u}) = \alpha_{i1} Y_1(\mathbf{u}) + \sigma_i U_i - \frac{1}{p} \sum_{l=1}^p \sigma_l U_l(\mathbf{u})$. Estimating $\Delta \log \Lambda_i$ by replacing Λ_i by a kernel estimate and the parameters by their conditional likelihood estimates, we obtain $\hat{Y}_1(\mathbf{u}) = (\hat{\alpha}^\top \hat{\alpha})^{-1} \hat{\alpha} [\hat{\Delta} \log \Lambda_1(\mathbf{u}), \dots, \hat{\Delta} \log \Lambda_p(\mathbf{u})]^\top$. The left plot in Figure 13 shows \hat{Y}_1 , where the Λ_i are estimated by kernel smoothing using a bandwidth of 3 km. There is some resemblance between $\hat{Y}_1(\mathbf{u}; h)$ and the spatial distribution of median income shown in the middle plot of Figure 13. Log median income is included as a covariate in the regression model for the log intensity. It may therefore be the case that $\hat{Y}_1(\mathbf{u})$ reflects nonlinear effects of the financial status of a neighborhood, cf. the right plot in Figure 13.

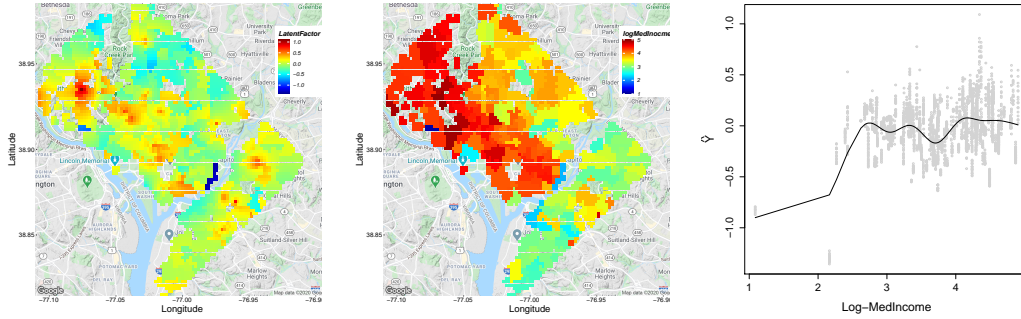


Fig. 13. Left: latent factor \hat{Y}_1 . Middle: log median income within census tracts. Right: \hat{Y}_1 versus log median income.

6. Conclusion

The methodology introduced in this paper provides a major step forward regarding second order analysis of multivariate point processes with complex intensity functions. Existing approaches (such as simple non-parametric estimation or the approach in Diggle et al., 2007) rely on estimating the intensity functions using kernel estimators. This tends to result in strong bias and/or large variance for subsequent estimation of PCFs and cross PCFs. In contrast, in the context of the model (3), our approach circumvents the need to estimate the complex unknown intensity function factor ρ_0 . According to our simulation studies, the resulting PCF and cross PCFs appear to be close to unbiased. For the data examples considered, we obtain simple and interpretable models that may result in better understanding of the interplay between respectively cells in tumors and different types of crimes.

A limitation of our approach, shared with existing methods, is that we have not provided confidence intervals for parameter estimates or confidence bands for estimated PCFs or cross PCFs. One topic for further research would be to estab-

lish asymptotic results for parameter estimates within the framework of estimating function inference. This was done by Hessellund et al. (2021) regarding inference for the intensity function but the current problem of inferring cross PCFs entail considerable additional theoretical difficulties.

The impact of using regularization was not very strong in our simulation studies when moderate values of q were considered. However, the crimes data example indicates that the use of regularization may add robustness to the estimation procedure if a too large q is selected.

The spatial crime point pattern data were obtained by aggregating data over consecutive two months. The implications of this particular choice of aggregation are not obvious. A highly interesting topic for further research would be to extend our methodology to a space-time analysis. One could e.g. envisage a space-time multivariate LGCP with latent common and type specific Gaussian fields evolving over time.

We finally mention that other useful cross summary statistics than cross PCFs are available for studying cross dependencies in inhomogeneous multivariate point processes. The inhomogeneous cross K -function (Møller and Waagepetersen, 2003) is basically a cumulative version of the cross PCF. Profoundly different cross summary statistics are the inhomogeneous cross empty space function, nearest neighbour distance function and J -function introduced in Cronie and van Lieshout (2016). As discussed in Section 11 in the supplementary material, the need to use an estimated intensity function ρ_0 complicates interpretation of results for these summary statistics. This is a topic that needs further investigation.

Acknowledgements

We thank Arnulf Mayer, Dept. of Radiation Oncology, University Medical Center, Mainz, Germany, for providing the fluorescence image and the point pattern data. Kristian B. Hessellund and Rasmus Waagepetersen were supported by The Danish Council for Independent Research — Natural Sciences, grant DFF - 7014-00074 ‘Statistics for point processes in space and beyond’, and by the Centre for Stochastic Geometry and Advanced Bioimaging, funded by grant 8721 from the Villum Foundation. Ganggang Xu was supported by NSF grant SES-1902195 and Yongtao Guan by NSF SES-1758575.

SUPPLEMENTARY MATERIAL

The supplementary material for this paper contains further plots, an algorithm for updating regularized α and auxiliary results.

References

- Baddeley, A., Jammalamadaka, A. and Nair, G. (2014) Multitype point process analysis of spines on the dendrite network of a neuron. *Journal of the Royal Statistical Society: Series C*, **63**, 673–694.

- Baddeley, A., Rubak, E. and Turner, R. (2015) *Spatial Point Patterns: Methodology and Applications with R*. CRC Press.
- Baddeley, A. J., Møller, J. and Waagepetersen, R. (2000) Non- and semi-parametric estimation of interaction in inhomogeneous point patterns. *Statistica Neerlandica*, **54**, 329–350.
- Choiruddin, A., Cuevas-Pacheco, F., Coeurjolly, J.-F. and Waagepetersen, R. (2019) Regularized estimation for highly multivariate log Gaussian Cox processes. *Statistics and Computing*, **30**, 649–662.
- Cronie, O. and van Lieshout, M. N. M. (2016) Summary statistics for inhomogeneous marked point processes. *Annals of the Institute of Statistical Mathematics*, **68**, 905–928.
- (2018) A non-model-based approach to bandwidth selection for kernel estimators of spatial intensity functions. *Biometrika*, **105**, 455–462.
- Diggle, P. J., Gómez-Rubio, V., Brown, P. E., Chetwynd, A. G. and Gooding, S. (2007) Second-order analysis of inhomogeneous spatial point processes using case-control data. *Biometrics*, **63**, 550–557.
- Guan, Y., Waagepetersen, R. and Beale, C. M. (2008) Second-order analysis of inhomogeneous spatial point processes with proportional intensity functions. *Journal of the American Statistical Association*, **103**, 769–777.
- Haberman, C. P. (2017) Overlapping hot spots ? examination of the spatial heterogeneity of hot spots of different crime types. *American Society of Criminology*, **16**, 633–660.
- Hastie, T., Tibshirani, R. and Friedman, J. (2013) *The Elements of Statistical Learning*. Springer Series in Statistics. New York, NY, USA: Springer New York Inc., 2 edn.
- Henry, P. and Brown, P. (2009) Inference for clustered inhomogeneous spatial point processes. *Biometrics*, **65**, 423–430.
- Herbst, R. S., Soria, J.-C., Kowanzetz, M., Fine, G. D., Hamid, O., Gordon, M. S., Sosman, J. A., McDermott, D. F., Powderly, J. D., Gettinger, S. N., Kohrt, H. E. K., Horn, L., Lawrence, D. P., Rost, S., Leabman, M., Xiao, Y., Mokatri, A., Koeppen, H., Hegde, P. S., Mellman, I., Chen, D. S. and Hodi, F. S. (2014) Predictive correlates of response to the anti-pd-l1 antibody mpdl3280a in cancer patients. *Nature*, **515**, 563–567.
- Hessellund, K. B., Xu, G., Guan, Y. and Waagepetersen, R. (2021) Semi-parametric multinomial regression for multivariate point pattern data. *Journal of the American Statistical Association*. DOI: 10.1080/01621459.2020.1863812.
- Jalilian, A., Guan, Y., Mateu, J. and Waagepetersen, R. (2015) Multivariate product-shot-noise Cox models. *Biometrics*, **71**, 1022–1033.

- Lavancier, F., Poinas, A. and Waagepetersen, R. (2019) Adaptive estimating function inference for nonstationary determinantal point processes. *Scandinavian Journal of Statistics*. Appeared online.
- van Lieshout, M. N. M. (2011) A J -function for inhomogeneous point processes. *Statistica Neerlandica*, **65**, 183–201.
- Møller, J. and Waagepetersen, R. (2003) *Statistical inference and simulation for spatial point processes*. Boca Raton: Chapman and Hall/CRC.
- Myllymäki, M., Mrkvička, T., Grabarnik, P., Seijo, H. and Hahn, U. (2016) Global envelope tests for spatial processes. *Journal of the Royal Statistical Society, Series B*, **79**, 381–404.
- Rajala, T., Murrell, D. J. and Olhede, S. C. (2018) Detecting multivariate interactions in spatial point patterns with Gibbs models and variable selection. *Journal of the Royal Statistical Society, Series C*, **67**, 1237–1273.
- Shaw, T., Møller, J. and Waagepetersen, R. (2020) Globally intensity-reweighted estimators for K - and pair correlation functions. *Australian and New Zealand Journal of Statistics*. Accepted for publication.
- Shi, P., Zhang, A. and Li, H. (2016) Regression analysis for microbiome compositional data. *Annals of Applied Statistics*, **10**, 1019–1040.
- Tibshirani, R. (1996) Regression shrinkage and selection via the Lasso. *Journal of the Royal Statistical Society, Series B*, **58**, 267–288.
- Tsujikawa, T., Kumar, S., Borkar, R. N., Azimi, V., Thibault, G., Chang, Y. H., Balter, A., Kawashima, R., Choe, G., Sauer, D., Rassi, E. E., Clayburgh, D. R., Kulesz-Martin, M. F., Lutz, E. R., Zheng, L., Jaffee, E. M., Leyshock, P., Margolin, A. A., Mori, M., Gray, J. W., Flint, P. W. and Coussens, L. M. (2017) Quantitative multiplex immunohistochemistry reveals myeloid-inflamed tumor-immune complexity associated with poor prognosis. *Cell Reports*, **19**, 203–217.
- Valkenburg, K. C., de Groot, A. E. and Pienta, K. J. (2018) Targeting the tumour stroma to improve cancer therapy. *Nature Reviews Clinical Oncology*, **15**, 366–381.
- Waagepetersen, R. and Guan, Y. (2009) Two-step estimation for inhomogeneous spatial point processes. *Journal of the Royal Statistical Society, Series B*, **71**, 685–702.
- Waagepetersen, R. P., Guan, Y., Jalilian, A. and Mateu, J. (2016) Analysis of multispecies point patterns by using multivariate log-Gaussian Cox processes. *Journal of the Royal Statistical Society, Series C*, **65**, 77–96.
- Weinberg, R. A. (2014) *The biology of cancer*. New York: Garland Science, Taylor & Francis Group.

- Weisburd, D., Maher, L., Sherman, L., Buerger, M., Cohn, E. and Petrosino, A. (1993) Contrasting crime general and crime specific theory: The case of hot spots of crime. *Advances in Criminological Theory*, **4**, 45–70.
- Xu, G., Waagepetersen, R. and Guan, Y. (2019) Stochastic quasi-likelihood for case-control point pattern data. *Journal of the American Statistical Association*, **114**, 631–644.
- Xu, G., Zhao, C., Jalilian, A., Waagepetersen, R., Zhang, J. and Guan, Y. (2020) Nonparametric estimation of the pair correlation function of replicated inhomogeneous point processes. *Electronic Journal of Statistics*, **14**, 3730 – 3765.
- Yan, Y., Leontovich, A. A., Gerdes, M. J., Desai, K., Dong, J., Sood, A., Santamaria-Pang, A., Mansfield, A. S., Chadwick, C., Zhang, R., Nevala, W. K., Flotte, T. J., Ginty, F. and Markovic, S. N. (2019) Understanding heterogeneous tumor microenvironment in metastatic melanoma. *PLoS One*, **14**. 0216485.
- Zou, H. and Hastie, T. (2005) Regularization and variable selection via the elastic net. *Journal of the Royal Statistical Society. Series B (Statistical Methodology)*, **67**, 301–320.